Asociación Argentina
de Mecánica Computacional

Mecánica Computacional Vol XXXIV, págs. 2063-2086 (artículo completo)
Sebastián Giusti, Martín Pucheta y Mario Storti (Eds.)
Córdoba, 8-11 Noviembre 2016

STUDY OF THE ROTOR-STATOR INTERACTION PHENOMENON IN A CENTRIFUGAL PUMP

Miguel G. Coussirat [a], Ricardo M. Aguirre [a], Leandro E. Panella [a] and Germán R. Henderson [a]

[a]*Grupo LAMA, Universidad Tecnológica Nacional, Facultad Regional Mendoza, Rodriguez 273, 5500 Ciudad Mendoza, Argentina, miguel.coussirat@frm.utn.edu.ar*

Keywords: Rotor-Stator Interaction, Unsteady Flow, Eddy Viscosity Models (EVM), Computational Fluid Dynamics (CFD), Pressure Fluctuations, Velocity Fluctuations, Scale-Adaptative Simulation (SAS).

Abstract. During operation of a turbomachine Rotor Stator Interaction phenomenon, RSI, appears in several cases. This phenomenon induces pressure fluctuations and it is closely related to the unsteadiness in the flow, which is highly turbulent, and due to the relative movements between moving and fixed parts of the machine. The induced pressure pulses and its oscillation frequencies could induce Flow-Structure Interactions, FSI, causing fatigue damages in the blades under certain conditions. The importance of the knowledge of the machine behavior under operation conditions that induces critical pressure pulses is of paramount interest, because the lifetime of the machine could be enhanced if this situation is suppressed. Computational Fluid Dynamics, CFD, is a powerful tool for studying the complex behavior of the flow that induces the RSI phenomena inside the machine, due to experimental options for studying this phenomenon are very expensive in these cases. But in some cases, due to the intrinsic unsteady nature of the RSI, the computational costs are very high if more sophisticated options are used (e.g., Large Eddy Simulations or Detached Eddy Simulations), becoming a prohibitive option for industrial flow modeling. In order to maintain the computational costs in an affordable level, in this work the main goal is to model the unsteady behavior by using a recently developed turbulence modeling option, related to the Scale-Adaptative-Simulation, SAS, applied to Eddy Viscosity Models, EVM. This option was selected, for searching an optimized use of the computational resources without loss accuracy in the details of the flow inside the machine.

1 INTRODUCTION

Nowadays, the trend in the imposed working requirements for hydraulic equipments in general, is an 'elastic hydrodynamic behavior' what means to cover several operation conditions during its exploitation. In many cases (e.g. hydraulic turbomachinery, valves, injectors, others) and under certain working conditions, the flow behavior inside the equipment leads to the apparition of complex phenomena such as a Fluid Structure Interaction, FSI, and a cavitating flow. Both phenomena are potentially dangerous because they provoke a low performance of the machine in its operation and the life of the equipment is shortened too.

The design of the hydraulic equipment that fulfills this elastic behavior requires a broader and deeper knowledge of the Mechanics science. It is broadly known that the branch of the Mechanics science called Computation Fluid Dynamics, CFD, is a useful tool in engineering design; but, to obtain accurate simulations of industrial flows it is necessary to assess the capabilities of the available numerical models for turbulence and cavitation. This assessment involves several calibration/optimization tasks based on the physics of these kinds of flow. Industrial engineers from companies involved in CFD tasks rarely spend enough time to perform these analyses, because it is broadly known that 'time is money' for companies. At present, collaboration between companies and universities are trying to 'fill this gap'.

It was mentioned that a good knowledge of the 'CFD environment' in complex flows involving turbulence and cavitation phenomena, implies a deeper understanding of several transport phenomena depicted by transport equations (mass, momentum, energy, turbulence and multi-phase mixture). It is possible to write them starting from each particular form (i.e., mass, momentum, energy, turbulence, etc. equation) in a generalized form, by introducing a general scalar $\boldsymbol{\phi}$ that represents the 'transported' property, and a subscript m that represents the 'mixture', i.e., the multiphase flow, see Li et al, 2008:

$$\frac{\partial \rho_m \phi_m}{\partial t} + \nabla \cdot \left(\rho_m \vec{c}_m \phi_m\right) = \nabla \cdot \left(\Gamma_m \nabla \phi_m\right) + S_{\phi,m}, \; \phi = \left\{1, \vec{c}, T, Y_j, k, \varepsilon, \ldots\right\} \tag{1}$$

Where $\boldsymbol{\rho}$ is the density, $\vec{c}$ is the velocity vector, $\boldsymbol{S_\phi}$ is a general source term, Γ_m is the diffusion coefficient; and $\boldsymbol{\phi}$ represents the dependent variables (scalars as the fluid temperature $\boldsymbol{T}$, the mass fraction for $\boldsymbol{j^{th}}$ species $\boldsymbol{Y_j}$, the turbulence kinetic energy $\boldsymbol{k}$, or its dissipation rate $\boldsymbol{\varepsilon}$; or vectorials as the velocity $\vec{c}$) in the system. It is highlighted again that the subscript $\boldsymbol{m}$ designates 'mixture', i.e., remarking that the fluid is a two- or multi- phase fluid. With the introduction of a cavitation model, the complete set of governing equations for turbulent cavitating flows can be derived from the foregoing generalized scalar transport equation.

Concerning the design of hydraulic turbomachines, it has reached the stage were improvements can only be achieved through a detailed understanding of the internal flow. The prediction of the flow in such equipment is here also very complex due to the aforementioned present phenomena (turbulence and cavitation), plus the rotation of the machine, and the curved three-dimensional shape of the impellers. Furthermore, the interaction between moving (rotor) and fixed (stator) parts in the machine, giving place to the RSI phenomena, a complex phenomena related to the inner flow in the machine, involving potential and turbulent effects due to the varying geometry of the flow passages into the machine. The flow in turbomachines ever shows unsteady behaviour, especially at off-design conditions, as a result of the interaction between impeller and vaned diffuser, i.e, RSI, and other interactions

e.g., rotor pump and casing, or vaned diffuser and casing. Considering these complexities, computer simulations will become increasingly important.

1.1 Common Strategies for Modeling the Turbulence

In order to define a turbulence model, the momentum equation (obtained from Eq.1 replacing ϕ_m by $\vec{c}$) is transformed by means of a special averaging, obtaining the Reynolds Averaged Navier Stokes equations, RANS, (also called Reynolds Averaged Simulations, RAS) where the turbulence fluctuations are set in an explicit form, giving place to a new term in this equation that recover the turbulence effects over the mean velocities. Then, this term is modeled by means of a turbulence model to transfer the effects provoked by the turbulent fluctuations into the computed mean flow (see details related to the given Refs. from Table 1 in Coussirat 2003 and Coussirat et al., 2016). This modeling gives place to the apparition of, e.g. k and ε variables in the generalized Eq.1, (or others depending on the turbulence model defined) when the variable ϕ is replaced by k and by ε. The aforementioned variables are typical variables of the broadly known **Standard k-ε** model.

Table 1: Turbulence models used, (see details of the references cited in this Table in Coussirat 2003 and Coussirat et al., 2016).

	Turbulence models	Notation	Reference
1	Spalart Allmaras	SA	Spalart and Allmaras [Spalart, 1994]
2	Standard k-ε	Std k-ε	Launder and Spalding [Launder, 1974]
3	Realizable k-ε	Rlz k-ε	Shi et al.[Shih, 1995]
4	Re Normalization Groups k-ε	RNG k-ε	Yakhot and Orzag [Yakhot, 1986]
5	Standard k-ω	Std k-ω	Wilcox [Wilcox, 1998]
6	Shear Stress Transport k-ω	SST k-ω	Menter, 1994 [Menter, 1994]
7	Reynolds Stress Model	RSM	Launder at al.[Launder, 1975]

Several modeling strategies for the turbulence are available nowadays, starting from model of zero equations towards models of one, two or four equations in the family of the Eddy Viscosity Models, EVMs, also so-called scalar models. More sophisticated ones are the Reynolds Stress Models, RSM, (so called tensorial models), and arriving finally to the more recent ones, the so-called Large Eddy Simulation, LES models, The latter models use quite a different strategy for averaging the Navier Stokes equations (spatial filtering, see Sagaut 2006), but this one also leads to a turbulence (or eddy) viscosity definition. Here, it is important to note that once a turbulence model is introduced into the momentum equations, these equations no longer carry any information concerning to their derivation (i.e., some kind of averaging technique). Both the RANS as well as the LES models are EVM that are used to substitute either the Reynolds- or the sub-grid stress tensor respectively. After the introduction of a turbulent (or eddy) viscosity, both the RANS and LES equations are formally identical. The difference lies exclusively in the turbulence scale represented by the eddy viscosity used/computed by the underlying turbulence model (see details in Menter and Egorov, 2010).

1.2 Common Strategies for Modeling the Cavitation

Also, it is very common to have cavitating flow in turbomachines adding more complexity for CFD simulations. Despite that the cavitation phenomenon is not studied in this work,

some brief details are given here taking advantage from the general structure of the already presented Eq.1.

In order to define a cavitation model in a general CFD code, a vapor transport equation is introduced since there is a process of liquid-vapor mass transfer for cavitating flows. It is considered that this liquid-vapor mass transfer process (evaporation and condensation) is governed by the following vapor transport equation, (see details in Li et al., 2008):

$$\frac{\partial \alpha \rho_v}{\partial t} + \nabla \cdot \left(\alpha \vec{c} \rho_v \right) = R_e - R_c . \tag{2}$$

Where α is the phase volume fraction, the subscript '$\boldsymbol{v}$' indicates the vapor phase; $\boldsymbol{R_e}$ and $\boldsymbol{R_c}$ are respectively the mass transfer source terms connected to the growth and collapse of the vapor bubbles. These terms account for the mass exchange between the vapor and the liquid phases during the cavitation process. Then, these terms can be modeled using the Rayleigh-Plesset equation (see details in Kubota et al., 1992, Singhal et al., 2002, Zwart et al., 2004, Franc et al, 2004, Kozubková et at., 2012) that describes the growth of a single vapor bubble in a liquid. The final set of Eq.2, Eq.3 and Eq.4 form the basis of several two-phase cavitation transport models included in several CFD codes after some manipulations, (e.g., see details in Li et al., 2008).

$$\frac{DR_B}{Dt} = \sqrt{\frac{2}{3}\frac{P_B - P}{\rho_l}}, \tag{3}$$

$$\frac{\partial \alpha \rho_v}{\partial t} + \nabla \cdot \left(\alpha \vec{c} \rho_v \right) = \frac{\rho_v \rho_l}{\rho_m} \frac{D\alpha}{Dt}. \tag{4}$$

Here, $\boldsymbol{R_B}$ is bubble radius; $\rho_l, \rho_v, \rho_m,$ are liquid, vapor and mixture densities; $\boldsymbol{P}$ and $\boldsymbol{P_B}$ are fluid and bubble surface pressures respectively.

1.3 Applying CFD for Turbomachinery Design

A general CFD code to apply to the modeling of a real turbomachinery comprises the set of all equations aforementioned. To solve this set of equations comprising turbulence and cavitation is a not trivial task, and it is necessary to take into account a lot of calibration parameters, together with the necessity of a careful validation of submodels (turbulence and cavitation ones). In order to perform the validation/calibration task, experimental databases are necessary and they are of paramount importance. Unfortunately, experimental measurements for turbulent cavitating flows in turbomachinery are very scarce because the major problem of physical experimentation is its high cost. In general, the experimental studies related to the vapor cavities structures present in the cavitating flow and their behavior are challenging due to the fact that cavitation is a very complex phenomenon and typically occurs in locations where the access to measuring instruments is limited; and it is also due to the presence of high velocities, high void fraction, and a considerable splitting of the dispersed phase (see details in Peters et al., 2015 and Duan et al., 2016). It is also necessary either to measure or to control a lot of parameters (i.e., local pressure and temperatures in the flow, the dissolved gases content, others). More complexity is added when, in some cases, cavitating flows start showing a periodic behavior in its development, strongly dependent on the fluid-flow state.

Similar observations concerning to the measurement difficulties can be made at the moment of take measurements of the unsteady turbulent flow pattern when different FSI phenomena are present in turbomachinery, e.g., to characterize the complete flow pattern, the boundary layer growing in the rotor or to measure fluctuating pressures when the RSI occurs between the rows of fixed and moving blades (see details in Pedersen et al., 2003 and Feng et al., 2011).

It is interesting to highlight that turbulence and cavitation are closely related. Turbulence affects cavitation inception since a nucleus may be found in the core of a vortex, where the local pressure level is lower than the mean value of the pressure in the flow. Hence, the nucleus could cavitate when it might not do so under the influence of the mean pressure level. This fact points out that cavitation may alter the global pressure field by altering the location of flow separation and the induced variations of the local turbulence level; thus, turbulence may promote cavitation and viceversa (see details in Coussirat et al., 2016).

Despite the fact that there are some general characteristics in several turbulent cavitating flows, the observed flow structures depend not only on the hydraulic device geometry but also on the fluid/flow parameters. Unfortunately, experiments provide detailed information 'case-by-case' only. For all the above mentioned reasons, CFD applied to this kind of flows is an active field of research and has significant importance for design engineers, because both turbulence and cavitation phenomena offer several challenges for a suitable modeling by means of the available CFD codes; and the moving reference frame, a tool commonly used for unsteady modeling of flow in turbomachinery, adds more difficulties to obtain credible CFD results.

2 VALIDATION/CALIBRATIONS TASKS, RESULTS AND DISCUSSION

To obtain a deeper knowledge of the available CFD codes capabilities for modeling complex flow in turbomachines, a brief summary of the work recently developed, where several modeling test cases studied using experimental databases, is presented here. The main goal of these works was to provide several quantitative criteria for suitable simulations in the branch of turbomachinery design. Using this previous experience, (see details in Fontanals 2012 and Coussirat et al., 2012) this work is focused on the study of the RSI phenomena and the set of cases selected here are related specifically to the RSI phenomena that appear in turbomachinery under normal or off-design operation conditions (a similar work focused to study the calibration of turbulence models for cavitating flows is also being performed). Details of the RSI phenomenon can be seen in the next section.

It was already mentioned that the RSI phenomenon is a complex flow involving potential and turbulent effects. In order to have a systematic approach to this complex phenomenon, simpler test cases than a real turbomachine, but closely linked to the RSI in the machine were selected for CFD modeling. These experimental databases are related to steady and unsteady flow around isolated airfoils/hydrofoils (see Fig.1, Fig.2 and Fig.3) and RSI in a cascade of moving blades, (see Fig.4). Several validation/calibration tasks were carried out to obtain information about the capabilities for modeling this kind of flows by means of the available turbulence models (see more details in Coussirat et al., 2008, Fontanals et al., 2011, Fontanals 2012, Coussirat et al., 2012, Guardo et al., 2013 and nd Fontanals et al., 2014).

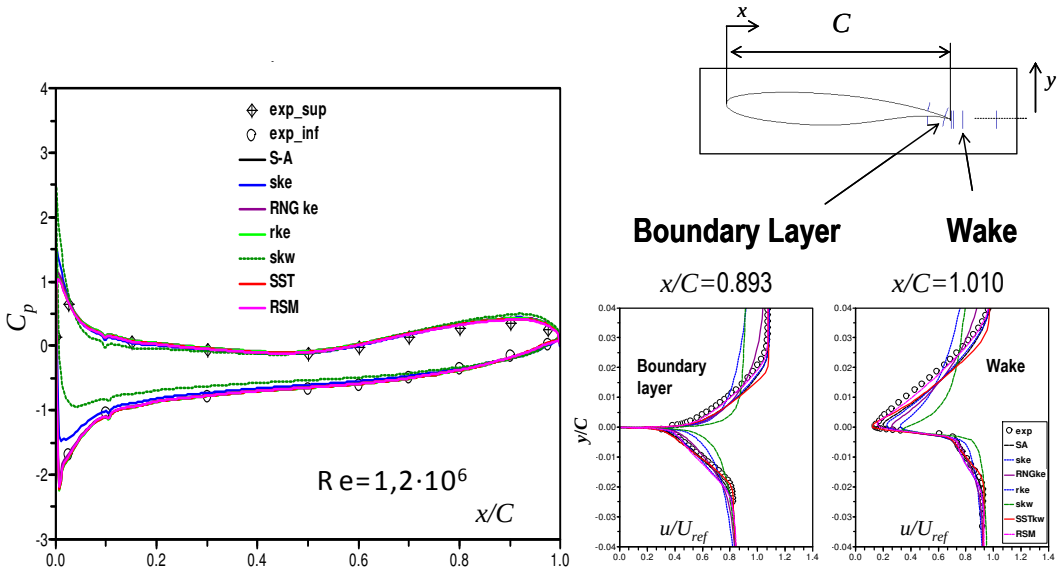

Fig.1: CFD Results for Boundary Layer and Wake flows over a supercritical profile airfoil: **Left**, pressure coef., C_p; **Right**, mean velocity, u. Experiments from Nakayama et al., 1985 (see reference and details in Fontanals 2012 and Coussirat et al., 2012). Nomenclature: x/C distance from leading edge of the hydrofoil/chord, $u/Uref$: local velocity value/mean velocity value.

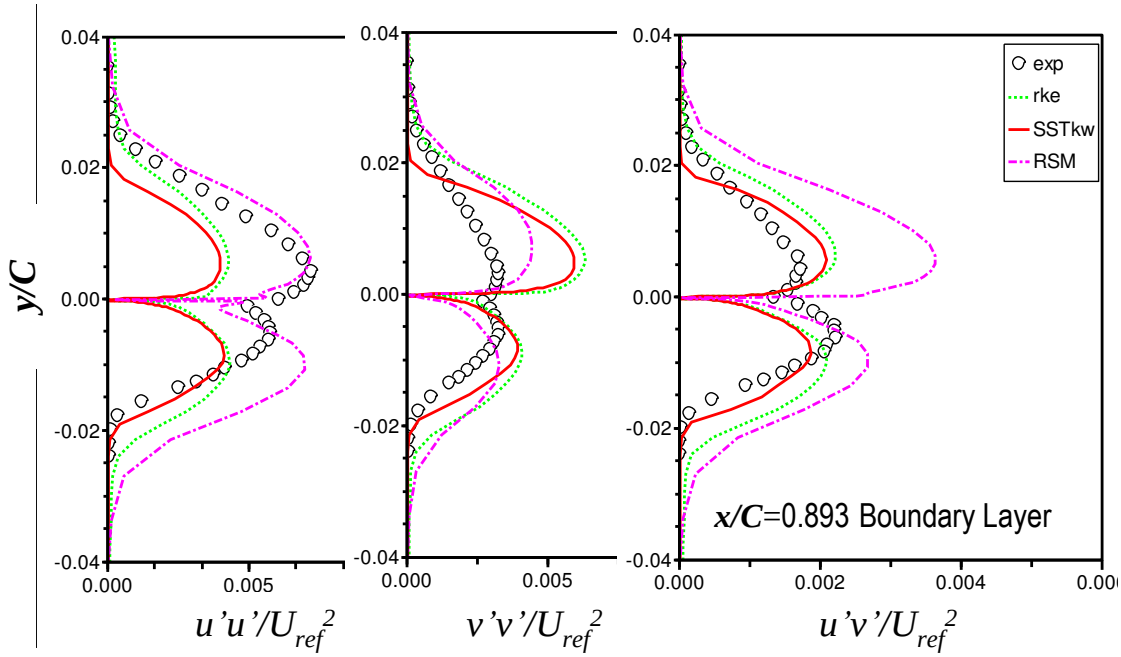

Fig.2. CFD Results for Boundary Layer flow around a supercritical airfoil: fluctuating velocities along the boundary layer. Experiments from Nakayama et al., 1985 (see details in Fontanals 2012 and Coussirat et al., 2012). Nomenclature: $x'x'/U_{ref}^2$: local fluctuation component / mean velocity value.

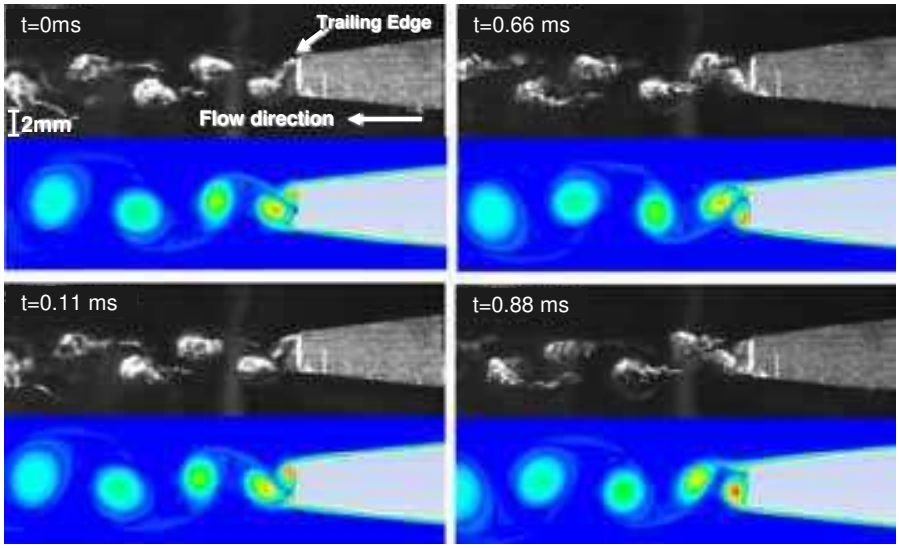

Fig.3. CFD Unsteady flow over a NACA 0009 truncated hydrofoil. Results obtained for the frequency of the von Kàrmàn vortex street, were compared against experiments from Ausoni et al. 2005 (B/W pictures), see details in Coussirat et al., 2012).

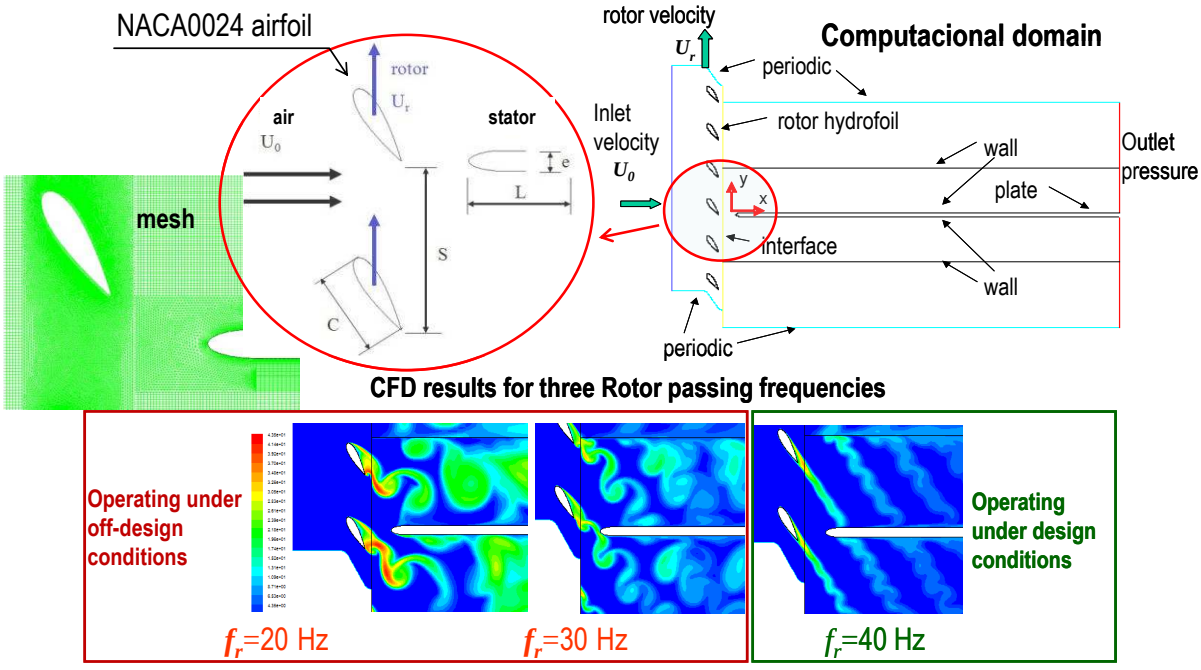

Fig.4. CFD Results for the RSI phenomena, Gette and Evans experiment. **Up:** mesh and geometry of the experimental setup for CFD. **Bottom:** Results obtained for different blade passing frequency, f_r=20Hz, 30Hz and 40Hz, (see reference and details Fontanals 2012 and Coussirat et al., 2012). CFD results obtained showed that depending on f_r, a different structure of the flow along the plate is present.

The main goal of these previous studies carried out and summarized here, was to observe the behavior of several EVM models (see Table 1) related to: a) reproduce the pressure coefficient C_p, the mean velocity field (see Fig.1) and its turbulent fluctuations (see Fig.2) for a steady fluid flow over a supercritical profile airfoil; b) reproduce the fluid flow field and the typical oscillation frequency in the wake (von Kàrmàn vortex street) for an unsteady flow over a NACA profile hydrofoil (see Fig.3); c) reproduce the boundary layer fluctuations along a plane plate (stator) and their characteristic oscillation frequencies due to the RSI phenomena in a cascade of moving blades (see Fig.4); d) reproduce the flow pattern in cavitating flows in injectors, Venturis and other hydrodynamic devices with simple geometry (results obtained in this last item are not shown in the present work).

All of these works allows to define a suitable CFD setup for subsequent RSI simulations in turbomachinery (geometry meshing, models selection, boundary layer definitions, discretization schemes, etc.), because several sensitivity tests related to the mesh size, cells distribution in the boundary layer, and the discretization schemes influence on the results, were performed (not shown here, see details in Fontanals et al., 2011). Also, some ideas about the capabilities of the different turbulence models used for recovering the detailed structure of these flow patterns were obtained by means of these previous simulations, obtaining several useful conclusions that are summarized here:

a) When a flow around a thin trailing edge isolated foil, or around a stage of fixed and moving cascade of blades was modeled, the **SST *k-ω*** turbulence model shows a good performance to compute the profile of velocities in the boundary layer and the general flow pattern of the wake; results obtained with others EVMs (see Table 1) do not show big differences in both cases. The fluctuating velocities u' in general were underestimated; but, v' and $u'v'$ fluctuations were overestimated for all the EVMs tested.

b) When a flow around a truncated (i.e., non thin trailing edge) isolated foil was modeled, the **SST *k-ω*** turbulence model shows a good performance to compute the velocity profiles along the boundary layer, and it also shows a slight overestimation of the shedding frequency.

c) When a flow around a stage of fixed and moving cascade of blades was modeled, the EVMs used shows underestimations of the turbulence intensity, $I\% = \sqrt{\overline{u'^2}}/U_0$, (where U_0 is a reference mean velocity) along the flat plane (stator), compared against experiments, as well as for isolated foils having thin trailing edges and low flow incidence angles.

d) In all the cases tested not big differences were observed in the results obtained by means of EVMs, DES or LES models, therefore it is possible to say that the main advantage of the EVMs is their low computational cost when compared to more accurate turbulence models (but more resource-consuming) such as the RSM or the LES (see details of these comparison in Coussirat et al., 2008, Fontanals 2012 and Guardo et al., 2013); being this fact of paramount importance when a flow in a complete turbomachine is modeled. On the other hand, and despite that the DES is an hybrid formulation between EVM and LES that need less computational resources than LES (but more than EVMs), some results obtained (not shown here) using DES allow to say that there is not a clear improvement compared to the results obtained by using EVMs.

2.1 Database Selected for Rotor Stator Interaction, RSI, Phenomena

It was aforementioned that in turbomachinery design, the RSI has a strong influence in the machine behavior and it is necessary to take it into account. It is not possible to do any prediction of this phenomenon by using classical theory for turbomachinery design, and to take into account its effects relies only in the designer experience. These interactions can have

a significant impact in the vibrational and acoustical characteristics of the machine, because unsteadiness and turbulence play a fundamental role in complex flow structures. The RSI can be divided into two different mechanisms: potential flow interaction and wake interaction. The nature of the flow due to the wake interaction is unsteady and turbulent, and there, three-dimensional (3D) boundary layers, curvature and system rotation effects (see more details in Fontanals et al., 2011) also appear. The choice of an appropriate turbulence model and the boundary layer treatment is far from trivial, and a suitable turbulence modeling plays an important role for successful CFD results, see Coussirat et al., 2008. The experimental data used here are for a single-stage pump with a specific number, n_q~53[rpm×(m^3/s)^{0,5}×m^{0,75}]; being a vaned diffuser pump with five impeller blades Z_i, eight diffuser vanes, Z_g and a volute casing as shown in Fig.5.

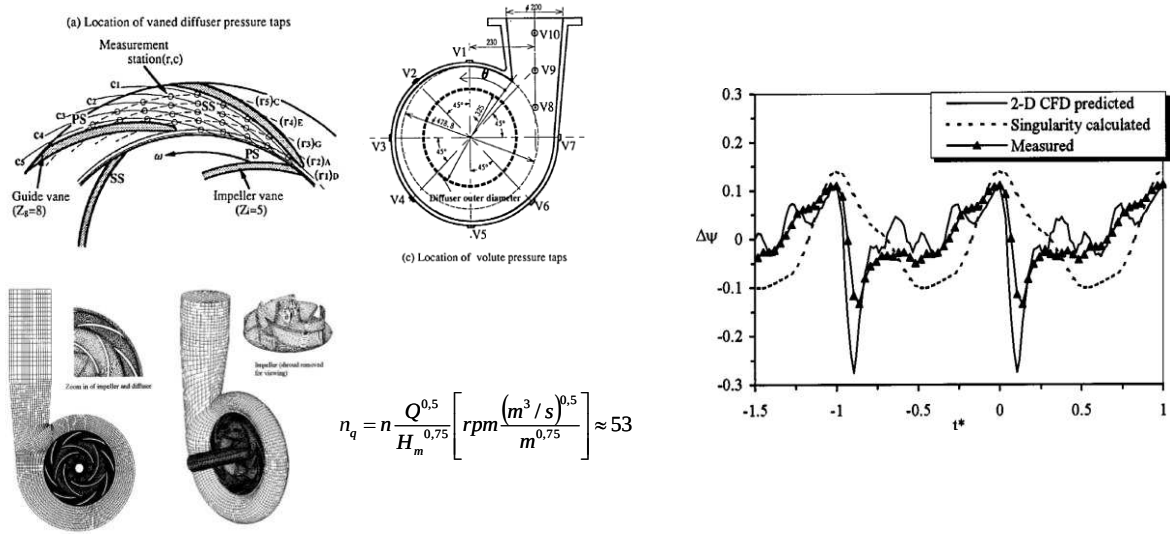

Fig.5. Experiments from Tsukamoto et al., 1995. Tested pump showing positions of the pressure measurement stations for the vaned diffuser and the locations of the volute pressure taps. Meshes and CFD results for pressure fluctuations showed correspond to 2D and 3D CFD cases from Shi et al., 2001. Nomenclature: $\Delta\psi$ = Unsteady pressure coeff. = p_{relat} ×(0.5ρU_2^2)$^{-1}$; U_2=peripheral speed of impeller (at its exit); t^*=non-dimensional time=t/T_i; T_i=time required to traverse one pitch of impeller blade.

A detailed description of the pump and its specifications of the essential components are summarized in Tsukamoto et al. 1995. The unsteady pressure measurements were made at several places (stations) in the vaned diffuser passage, and a comprehensive survey of the unsteady pressure field within the diffuser passages was obtained. Fig.5 also illustrates the unsteady pressure measurement stations in the shroud casing side of the diffuser in the test pump.

The unsteady pressures were measured by semi-conductor-type pressure transducers, which were installed directly on the pressure taps to prevent the decrease of natural frequency in the pressure measurement systems. Due to the limited space in the measuring sections, the pressure taps for tangential traverse were located at one radial location in each passage of the diffuser only. The blade-to-blade distributions of unsteady pressure were identified by a phase shift of the measured data. The coordinates of the static pressure taps were formed by the cross of five radial grid lines and five stream-wise grid lines in a blade-to-blade passage as shown in Fig.5.

3 CFD FOR THE TURBOMACHINE UNDER THE DESIGN CONDITION

In order to explore the Scale-Adaptative-Simulation, SAS, option together with the EVMs, a discussion based in the previous results obtained by the authors using EVMs is given here. This discussion is related to the actual possibilities of the EVMs applied to model the RSI phenomena in turbomachinery working both under normal conditions (design condition) and under off-design conditions, (see Fontanals et al., 2011, Fontanals, 2012, Coussirat et al., 2012 and Guardo et al., 2013 for more details).

In all the cited cases, and for the design condition, the set of Two dimensional, unsteady incompressible Reynolds-averaged Navier-Stokes equations were solved by means of the commercial CFD code Ansys Fluent 12.1. An entire 2D stage of a diffuser pump was modeled to study the pressure fluctuations due to the interaction between the impeller and the diffuser of the pump. Unsteady fluctuations of pressure in the steady vane and frequencies of the pressure fluctuations in the diffuser passage were computed and compared against experimental results from Tsukamoto et al., 1995. Full RANS equations coupled with several EVMs (see Table 1) were solved for the 2D stage to establish the most accurate modeling strategy for a diffuser pump. A constant pressure value was imposed at the fluid inlet and a constant pressure value was imposed at the pump outlet. These values were obtained from the characteristic curve of the pump (see mode details in Tsukamoto et al., 1995), checking that the maximum efficiency is obtained at this point, i.e., working under the design condition.

A non slip boundary condition was imposed in the runner blades, diffuser vanes and volute casing wall. A rotational speed, $\boldsymbol{N}$, of 2,066 rpm was imposed to the blade impeller implying that this validation/calibration study is made for the turbomachine working under design conditions (optimal performance). Applying the aforementioned previous experience concerning to turbulence in blades and cascade of blades, an entire 2D stage of a diffuser pump was modeled to accomplish the proposed turbulence model performance study. The setup defined for this case consists in an unsteady simulation including a second-order implicit velocity formulation and a pressure-based solver. The SIMPLE pressure-velocity coupling algorithm was used, and a second order scheme discretization was selected for the numerical experiments.

The maximum number of iterations for each time step was set to 40, to reduce all computed normalized numerical residuals till an order of $O(10^{-5})$. The interface between the rotor blade and the diffuser vane was set to a sliding mesh, in which the relative position between the rotor and the stator was updated every time step. The adopted computational time step was about 1/360 of the rotor revolution time. Due to the unsteady nature of the flow, it is required that the whole flow domain be affected by the unsteady fluctuations. In order to check the aforementioned situation, a flow rate monitoring was made at the domain outlet. After starting the simulation, the machine must spin some time while the flow pattern is computed to obtain the uniform unsteady flow and then, check the uniformity in the shape of pressure fluctuations; uniform unsteady flow behavior was obtained after 10 revolutions.

For checking the performance of the turbulent models from Table 1, the results obtained for pressure fluctuations in three monitoring points $\boldsymbol{r_1c_1}$, $\boldsymbol{r_1c_3}$ and $\boldsymbol{r_2c_3}$ of the vaned diffuser passage were recorded for every numerical simulation developed. These points correspond to the reported measurement points for the experimental data set from Tsukamoto et al., and their location can be seen in Fig.5 and Fig 6.

In order to capture the RSI effects, the relationship between the pressure fluctuations and the movement of the rotor vanes in front of the diffuser vanes was extracted from the

computed unsteady pressure field. Using a Fourier transform, the characteristic frequencies of the pressure fluctuations were obtained at points r_1c_1, r_1c_3 and r_2c_3.

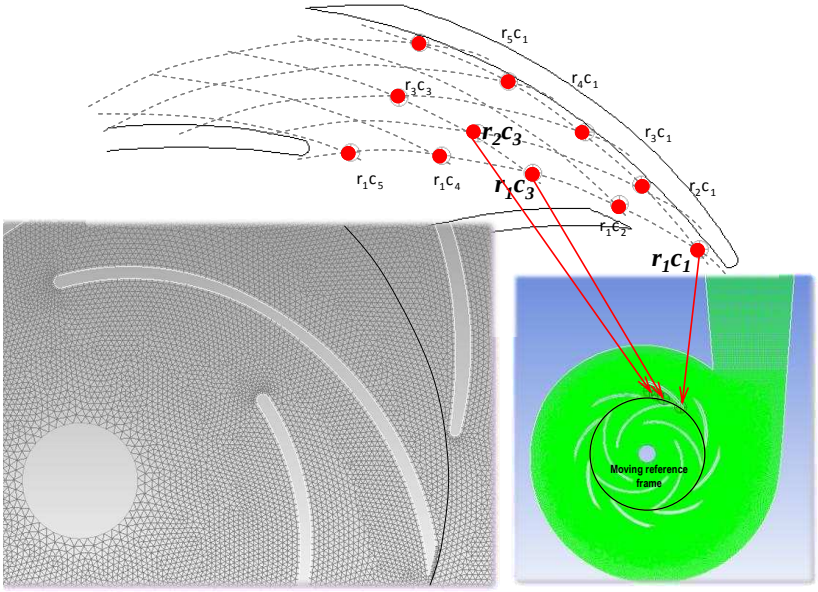

Fig.6. Details of the meshed geometry for a diffuser pump. Notation: $r_i c_i$, i=1-5, places where the unsteady pressures were measured (Tsukamoto et al., 1995).

In Fig.7 the results obtained for the pressure fluctuations at r_1c_3, showing that the pressure fluctuates with the impeller blade passing frequency Z_iN and its higher harmonics can be seen, (more details in Fontanals et al., 2011, Fontanals, 2012, Coussirat et al., 2012 and Guardo et al., 2013).

After that, a detailed analysis of the obtained results allows to notice that using a mesh with y^+~25 (i.e., first cell center at a distance of y^+~25 from the wall) the Spalart-Allmaras, the **Rlz** k-ε and the **SST** k-ω turbulence models show the best adjustment for the experimental pressure fluctuations (see Fig.8). This mesh is also suitable to use Wall Functions, WF, for turbulence models that need this kind of near-wall treatment.

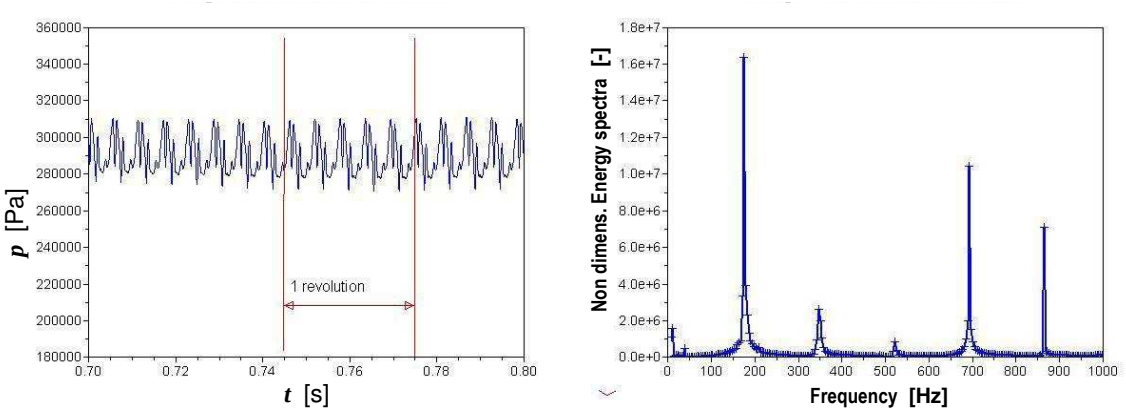

Fig.7. CFD results for design conditions, (Q=1,0Q_d) for the Spalart-Allmaras model. **Left**, CFD results for the pressure fluctuations at point r_1c_3 (see Fig.5); **Right**, frequency domain showing the harmonics of the unsteady pressure fluctuations obtained from the CFD computations.

Similar results were obtained for refined meshes, (i.e. y^+~5), requiring a Two-Layer Modeling, TLM, for the near-wall treatment for some turbulence models (not shown, see details in Fontanals et al., 2011, Fontanals, 2012, Coussirat et al., 2012 and Guardo et al., 2013).

It can be noticed that both the **Std *k-ω*** as well as **SST *k-ω*** turbulence models have some difficulties to capture some of the representative frequencies of the fluctuations, while all the other models tested, accurately capture the characteristic frequencies of the phenomena (see full details in Table 3 from Fontanals et al., 2011).

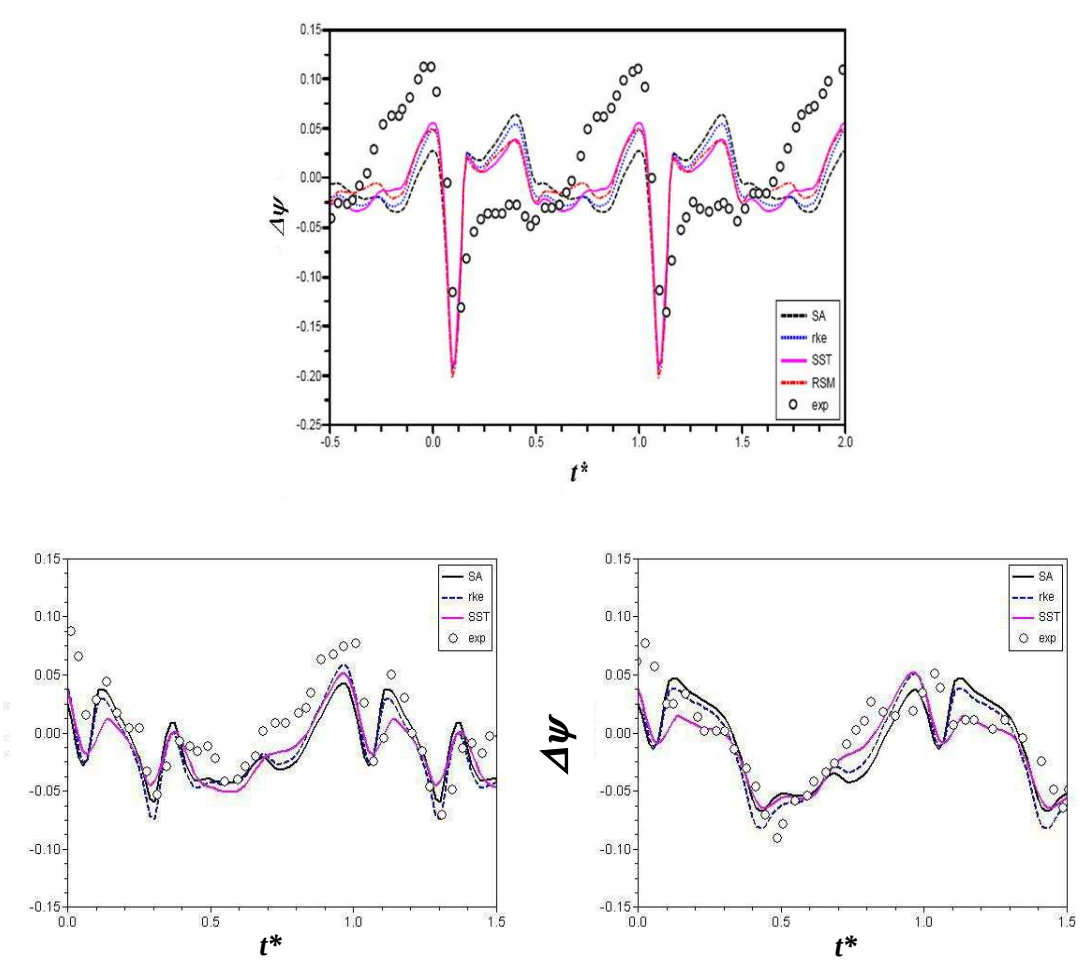

Fig.8. CFD results using a mesh with y^+~25 and several turbulence models.
Up: point r_1c_1, from Guardo et al., 2013. **Bottom-Left,** point r_1c_3; **Bottom-Right,** point r_2c_3. $\Delta\Psi$ vs t^*, from Fontanals 2012.

An interesting result is that it could be possible to recover the unsteady signal from the frequency spectra obtained, allowing to separate the potential and viscous effects. Since the potential effect can be recovered applying a typical theoretical frequency analysis, see Rodriguez et al., 2007, a subsequent subtraction of the potential effect from the total signal obtained by CFD computation (potential+turbulence) would permit the recovering of the turbulence effect, (see Fig.8 and Fig.9). This idea could be useful to analyze turbulence spectra or which frequency affects more the pressure fluctuations.

On the other hand, the analysis of the associate velocity field to the pressure fluctuations is

of great interest in order to understand RSI phenomenon more completely. Unfortunately, the Tsukamoto database has only pressure fluctuations measurements and there is no information about the velocity field. Despite this fact, the velocity field was computed and compared qualitatively against similar experiments from Pedersen et al., 2003 and experimental/CFD results from Feng et al., 2011 to obtain a more complete idea about the capabilities of CFD to reproduce the flow pattern, see Fig.10 and Fig.11).

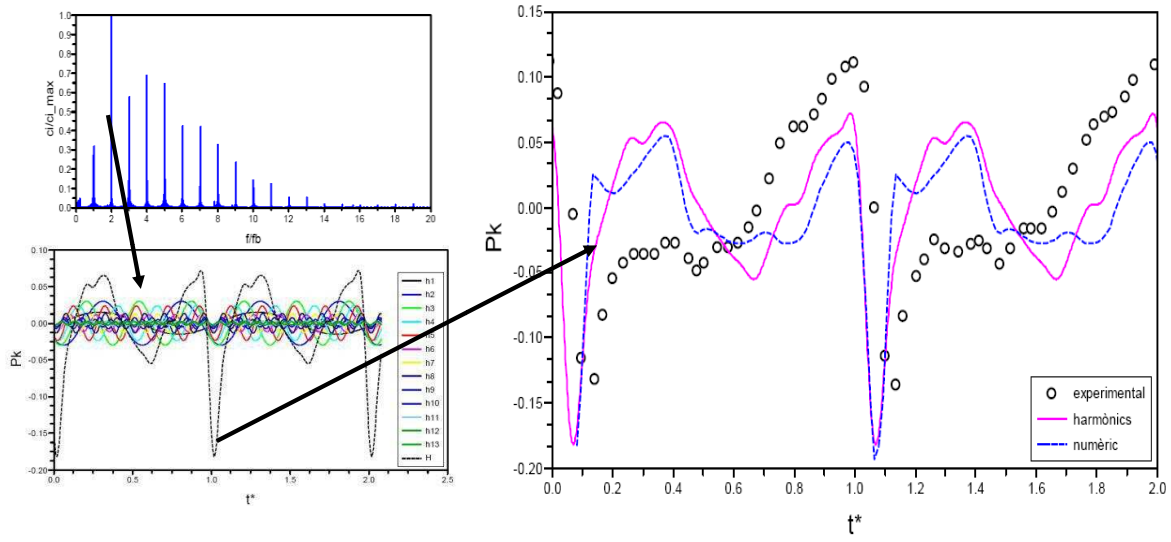

Fig.9. CFD results using for design conditions, ($\boldsymbol{Q}$=1,0$\boldsymbol{Q_d}$) for the $\boldsymbol{r_1c_1}$ position (see Fig.8 Up). From the frequency spectra obtained by CFD it is possible to recover the complete (potential+turbulence) unsteady signal. The arrows point out the composition process for obtaining the complete signal starting with individual frequencies by means of their addition.

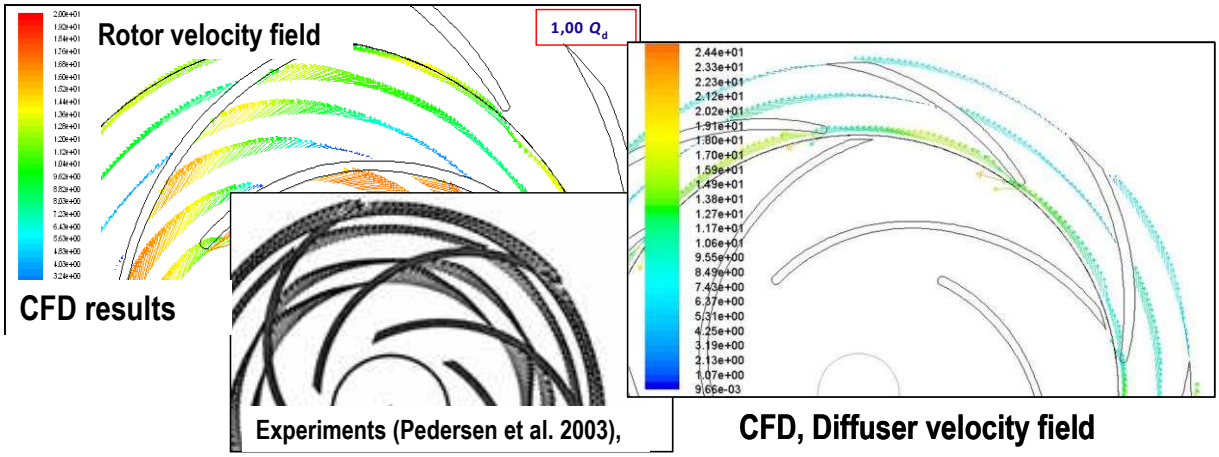

Fig.10. CFD results using a mesh with $\boldsymbol{y^+}$~25 for design conditions ($\boldsymbol{Q}$=1,0$\boldsymbol{Q_d}$). **Left,** rotor velocity field; **Right**, diffuser (stator) velocity field. Notice that quantitatively, the velocity field is similar as one from Pedersen et al., 2003. This database corresponds to a centrifugal pump without diffuser.

Fig.10 shows the velocity field obtained for the Tsukamoto et al., centrifugal pump both for the rotor as well as for the stator. The CFD results obtained for the rotor were compared to qualitatively against the experimental results for a centrifugal pump without diffuser vanes from Pedersen et al., 2003, showing similar velocity distributions in the rotor. The potential

effect in the rotor vane is clearly observed, and the structure of the boundary layers along the pressure side and the suction side of the blades was observed too.

Fig.11 shows comparisons of the relative velocity components along the pump vanes, against the experimental/numerical database for a centrifugal pump with a vaned diffuser from Feng et al., 2011. The comparison show similar flow field configuration, i.e., similar results were obtained despite that only the general shape of the velocity fluctuations can be compared because this pump has a lower n_q value than the CFD modelled Tsukamoto pump (see more details in Fontanals, 2012, Coussirat et al., 2012 and Guardo et al., 2013).

After these validations, it is possible to correlate pressure and velocity fluctuations in order to a better knowledge of the internal flow in the pump, and some conclusions were obtained. All the models tested showed good results for the pressure fluctuations in the vaned diffuser when compared against experimental results from Tsukamoto et al., except the **Std** k-ω model. It is possible to notice that the Spalart-Allmaras, **Rlz** k-ε and **SST** k-ω turbulence models show better adjustments than other EVM for the experimental pressure fluctuations, see Fig.8 Top, and more details in Fontanals, 2012, Coussirat et al., 2012 and Guardo et al., 2013.

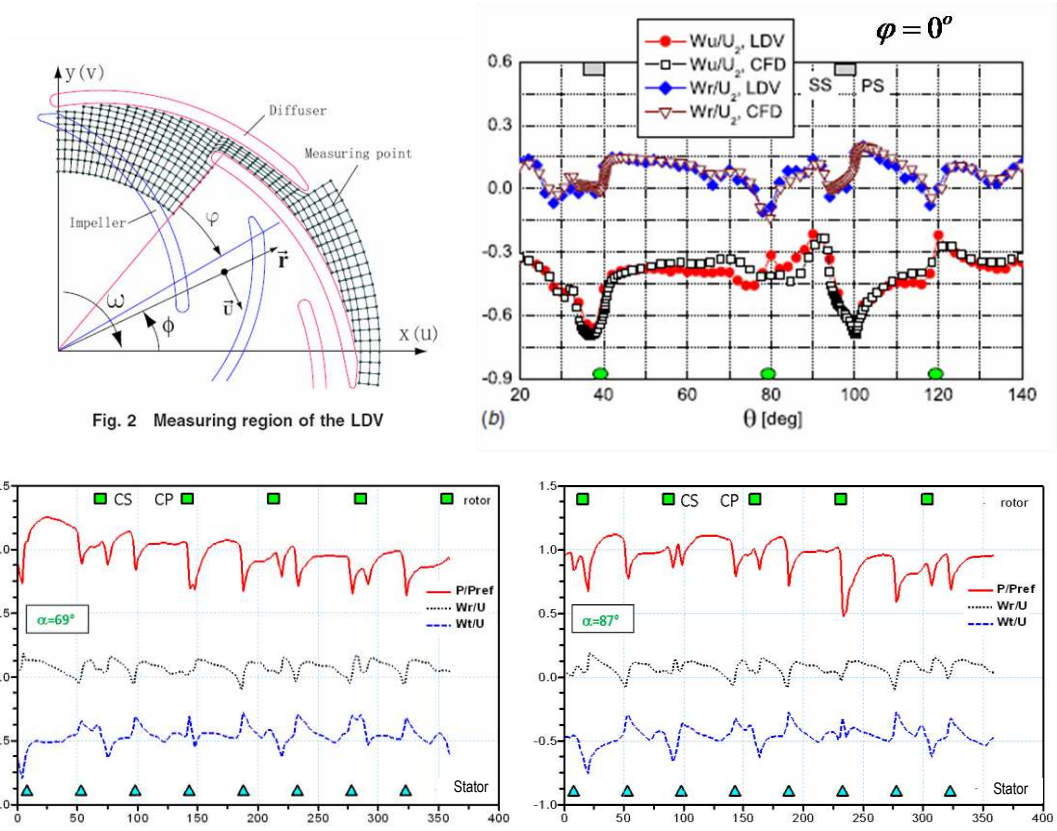

Fig.11. CFD results: velocity field for a radial machine, n_q~22[rpm×(m^3/s)$^{0.5}$×m$^{-0.75}$], Feng et al., 2011. **Top-Left:** Impeller configuration. **Top-Rigth:** Velocity field, rotor vane for design condition, (Q=1,0Q_d) and position φ=0^o, from Feng, (impeller rotation: from left to right). The circumferential positions of the impeller blades and diffuser vanes are marked at the top and bottom of the figure, respectively. **Notation:** LDV Laser Doppler Velocimeter measurements; **Wu**, tangential component of the relative velocity; **Wr**, radial component of the relative velocity. **Bottom:** CFD results obtained for Tsukamoto pump (pressure and velocity field vs circumferential position 0-360^o) for two relative stator-rotor positions (α). Notation: P_{ref}=p_{relat} , U=U_2.

When the influence of the boundary layer treatment applied on the results is analysed, it can be observed that meshes with y^+~25 are able to reproduce the RSI pressure fluctuations accurately, despite the fact that they do not allow to recover the boundary layer flow in detail.

Summarising, a general conclusion from the CFD results obtained for a vaned pump working under design conditions is that the relationship between the pressure fluctuations and the movement of the rotor vanes in front of the diffuser vanes was well determined. The characteristic frequencies of the pressure fluctuations were obtained, resulting that the pressure fluctuates with the impeller blade passing frequency Z_iN and its higher harmonics as the experiments show. All the turbulence models tested showed a periodic pattern in the pressure fluctuation in which each cycle is produced by the movement of a rotor blade in front of a diffuser vane, except for the **Std *k-ω*** and the **SST *k-ω*** turbulence models. For these two models, the pressure fluctuations values were different from each pass of an impeller blade in front of a diffuser blade, but the overall behavior for one revolution of the impeller followed a regular pattern.

Despite the difficulties found to capture all the frequencies of the pressure fluctuations (only the $2Z_iN$ was not well captured), the promising behavior of the **SST *k-ω*** model could lead to future unsteady simulations by using the Scale Adaptive Simulation, SAS, option, available for this turbulence model, (see a brief summary of its formulation in Eqs.5-8 and full details in Menter et al., 2003, Menter et al., 2010 and Egorov et al., 2010). The SAS option is a recent development related to unsteady turbulence modeling, and it is an improved Unsteady Reynolds Averaged Navier Stokes, URANS, formulation, which allows the resolution of the turbulence spectrum in unstable flow conditions.

Contrary to the standard URANS, SAS provides two independent scales for the source terms of the underlying two equations model, Eqs.5-8 (e.g., **SST *k-ω*** model). In addition to the standard input for the length scale in form of a velocity gradient tensor $\partial U_i / \partial x_j$, SAS model computes a second length scale, called the von Kàrmàn length-scale, L_{vK} from the second derivative of the velocity field, Eq.8. The information provided by L_{vK} allows the model to react more dynamically to capture scales in the flow field which cannot be handled by standard URANS models, because URANS recovers only the large-scale unsteadiness, whereas the SAS-**SST *k-ω*** model adjusts to the already resolved scales in a dynamic way and allows the development of a turbulent spectrum in the detached regions.

As a result, SAS offers a single framework, which covers steady state regions (computed normally by RANS) as well as unsteady detached flow regions (which must be computed by LES to solve their details), without an explicit switch in the model formulation, see details in Menter et al., 2010 and Egorov et al., 2010. Then, SAS would allow studies of unsteady flow behavior by means of an Unsteady RANS simulation including a technique for adapting the length scales automatically (SAS-URANS) instead of the more expensive, in terms of CPU requirements, LES option. The SAS-URANS option can be a very interesting engineering tool, since LES modeling for turbulent flows in complex geometries (industrial flows) are not affordable nowadays, see more details in Coussirat et al., 2012 and Coussirat et al., 2016.

$$\frac{\partial pk}{\partial t}+\frac{\partial}{\partial x_i}(\rho u_i k)=G_k-\rho c_\mu k\omega+\frac{\partial}{\partial x_i}\left[\left(\mu+\frac{\mu_t}{\sigma_k}\right)\frac{\partial k}{\partial x_i}\right] \tag{5}$$

$$\frac{\partial p\omega}{\partial t}+\frac{\partial}{\partial x_i}(\rho u_i \omega)=\alpha\frac{\omega}{k}G_k-\rho\beta\omega^2+Q_{SAS}+\frac{\partial}{\partial x_i}\left[\left(\mu+\frac{\mu_t}{\sigma_\omega}\right)\frac{\partial \omega}{\partial x_j}\right]+(1-F_1)\frac{2\rho}{\sigma_{\omega,2}}\frac{1}{\omega}\frac{\partial k}{\partial x_j}\frac{\partial \omega}{\partial x_j} \tag{6}$$

$$Q_{SAS}=\max\left[\rho\eta_2 kS^2\left(\frac{L}{L_{vK}}\right)^2-C\frac{2\rho k}{\sigma_\theta}\max\left(\frac{1}{\omega^2}\frac{\partial\omega}{\partial x_j}\frac{\partial\omega}{\partial x_j},\frac{1}{k^2}\frac{\partial k}{\partial x_j}\frac{\partial k}{\partial x_j}\right),0\right] \tag{7}$$

$$L_{vK}=\max\left(k\left|\frac{U'}{U''}\right|,C_S\sqrt{\frac{k\eta_2}{(\beta/c_\mu)-\alpha}}\cdot\Delta\right),\Delta=\Omega_{CV}^{1/3} \tag{8}$$

In summary, the functionality of SAS is similar to the Detached Eddy Simulations, DES, being DES a hybrid formulation that uses both EVM and LES. The LES activity in DES is enforced by the grid limiter, whereas SAS allows a breakdown of the large unsteady structures by adapting the turbulence model to the locally resolved length scale. This functionality could be explored more extensively to open the possibility to perform unsteady CFD simulations with affordable CPU costs not using so big computational meshes.

At the moment, the SAS option is coupled to the **SST *k-ω*** model in Ansys Fluent v12.1, and for this reason the behavior of the **SST *k-ω*** model was observed carefully, analysing its performance in the previous works. Afterwards, the SAS option was explored in this work and some results obtained are presented in Fig.12.

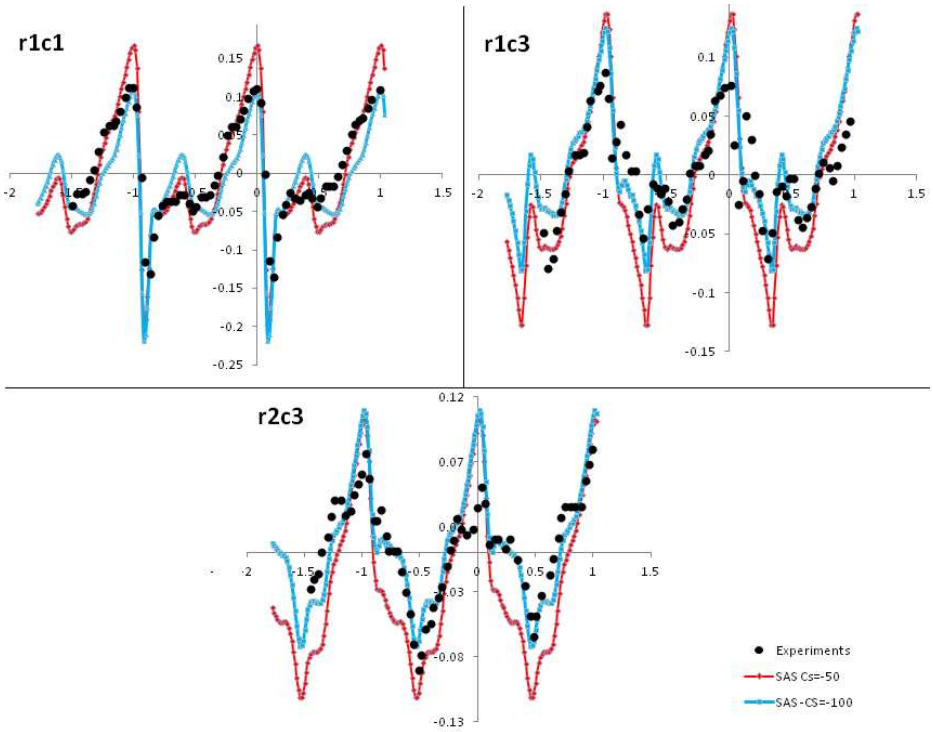

Fig.12. CFD results for the non-dimensional head-flow rate, $\Delta\psi=(2gH_mU_2^2)$ vs ***t****. **Up-left**: r_1c_1 position; **Up-Right**: r_1c_3 position; **Down**: r_2c_3 position. Nomenclature: • Experimental data from Tsukamoto et al., 1995.

The results obtained here were compared against the previous ones obtained using several EVMs, including the **SST *k-ω*** model, (see Fig.8) and against the experimental results from Tsukamoto for the vaned diffuser pump working under design conditions.

Like others EMVs, the SAS model has several parameters for its calibration. One of paramount importance is the C_s parameter, see Eq.8. This parameter has a control over the L_{vk} scale allowing the model to react more or less dynamically, and in this way it is possible to recover more or less unsteady effects.

Fig.12 shows a comparison among the results obtained using the SAS model, with some calibration of the C_s parameter. The results obtained show that by a suitable calibration of SAS (the default value for C_s is 0.11), it is possible to adjust very well the positive pressure peaks (Fig.12**,** Up-Left) in a better way at the r_1c_1 position, i.e., near of the leading edge of the stator blade, just when the flow from the rotor goes into it (see Fig.6). Also, the general shape of the fluctuation is quite good adjusted, but the negative peaks are not well predicted. Similar results are obtained for the positions r_1c_3 and r_2c_3, but here, the negative pressure peaks are betted predicted, instead of the positive ones. A comparison of the results obtained with SAS (Fig.12) against ones obtained using other EVMs (Fig.8) shows that a better general adjustment is obtained by means of SAS in all cases.

In Fig.13 a more detailed comparison between the results obtained using the SST ***k-ω***, and the 'calibrated' SAS models, showing that a general improvement of the shape of the pressure fluctuation at the position r_1c_1 was obtained. A better fitting of the positive pressure peaks were obtained with SAS too. Instead, at positions r_1c_3 and r_2c_3 better fitting were obtained for the negative pressure peaks by using SAS, but positive pressure peaks were overestimated.

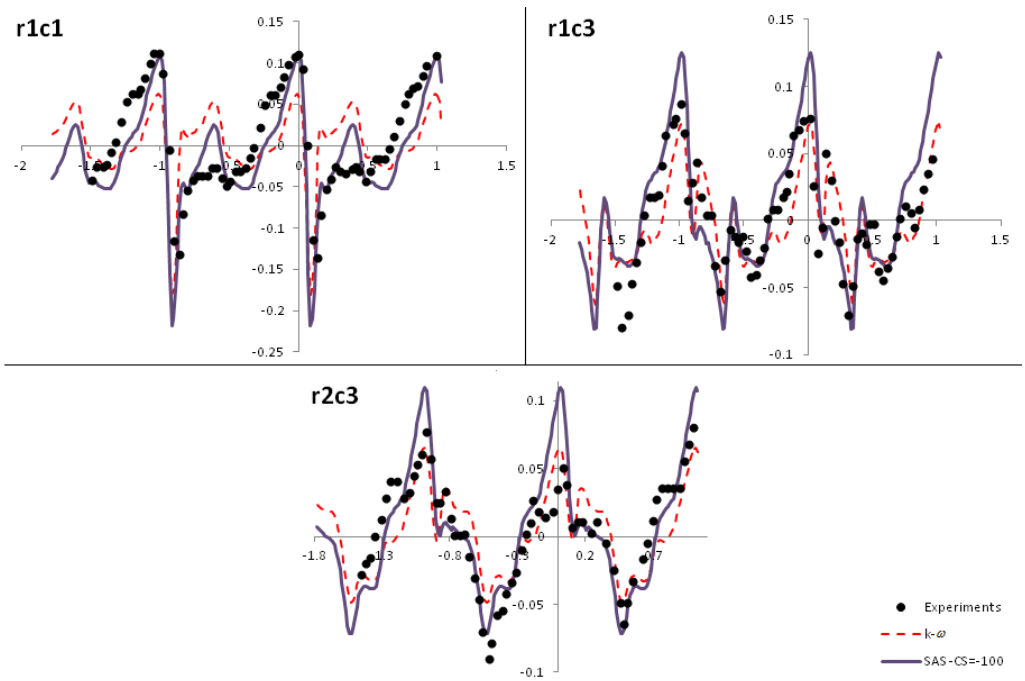

Fig.13. CFD results for the non-dimensional head-flow rate, $\Delta\psi=2gH_mU_2^2$ vs t^*.
Up-left: r_1c_1 position; **Up-Right**: r_1c_3 position; **Down**: r_2c_3 position. Nomenclature: • Experimental data, Tsukamoto et al., 1995, --- **SST *k-ω***, **— SAS** (C_s= -100).

As a conclusion of the results obtained by means of SAS, it is possible to say that a general improvement of the shape for pressure fluctuations was obtained, by comparing these results against ones obtained by EMVs. The fact that positive pressure peaks were better adjusted than the negatives ones at the r_1c_1 position, could be attributed to the fact that at positions near of the wall, the viscous effects are of the same intensity as turbulent ones. The opposite effect was observed at r_1c_3 and r_2c_3 positions, being both positions far of the wall.

4 CFD FOR THE TURBOMACHINE UNDER OFF-DESIGN CONDITION

Bearing in mind the already presented validation/calibration work, now it is possible to select better options for a subsequent CFD study for this turbomachine working under off-design work conditions, being this subject other goal of this work.

Despite that an experimental database for off-design conditions is not available for this case, it is interesting to highlight that after an extensive validation/calibration of the models it is possible to 'extrapolate the models performance', but carefully, to obtain new results when the machine is working under off-design conditions. It is necessary to remark that these conditions provoke an enhancement of the boundary layer thickness and the possibility of flow detachment becomes possible, being a challenge for the EVMs without any calibration.

The knowledge of the behavior of the turbomachine working under off-design conditions is of paramount importance for design engineers, and to obtain credible trends in its behavior by means of CFD becomes an interesting option to explore. By varying the flow rate, and defining the suitable head, some results were obtained for off-design conditions, see Fig.14, where the results obtained for several cases are shown, (marked with squares). Different conditions were defined by means of changing the boundary conditions to simulate the turbomachine working under design or off-design conditions. Notice that if the machine was working under the design point, the mean value for the pressure (non dimensional value ψ) is well captured by the CFD simulation.

The enhancement of secondary flows under off-design operating conditions provokes strong secondary flows that affect the boundary layers thickness and their structure leading to an increase of the turbulence level. To manipulate this flow condition is very hard for EVM, and SAS option could become an interesting one, because LES option is very consuming in terms of CPU resources. Some details of the fluid flow under design and off-design work conditions can be seen in Fig.14. Notice that the CFD adjustments of the curve for off-design conditions go down, but the trend is well reproduced.

Then, by means of CFD it is possible to observe details of the complex flow in the turbomachine that sometimes is very hard to obtain by means of experiments. Fig.14 also shows that under off-design operation conditions secondary flows and instabilities appear in the rotor, affecting the general flow pattern.

These perturbations are convected to the rotor outlet and then, start affecting the stator flow into the channels, leading to a 'stalling cycle' in the channel. This 'stalling cycle' has a completely unsteady behavior that affects the general performance of the machine. In some cases, and depending on de local flow behavior, a cavitating flow can appear too.

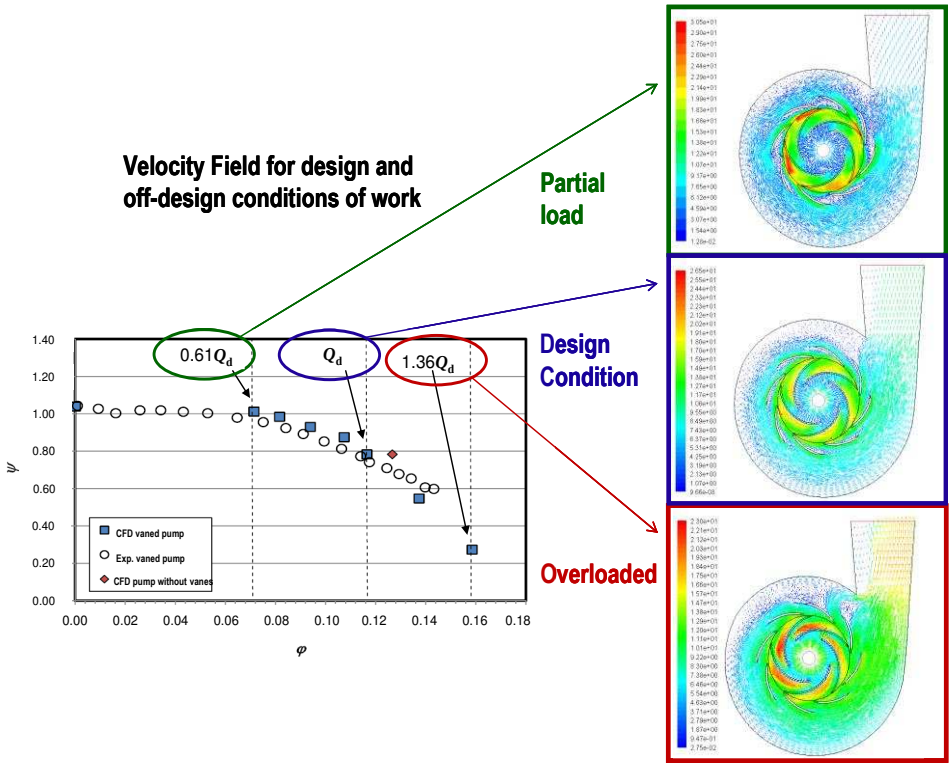

Fig.14. CFD results, (ψ, φ) **Left**: curve for the vaned pump; **Rigth:** Assocciated fluid flow pattern for some working conditions. Notation: Non-dimensional head-flow rate curve ($\Delta\psi$, $\Delta\varphi$); pressure coeff., $\Delta\psi=(2gH_mU_2^{-2})$; flow rate coeff., $\Delta\varphi=(Q)\times(2\pi b_2R_2U_2)^{-1}$; o, Exp. from Tsukamoto et al., 1995.

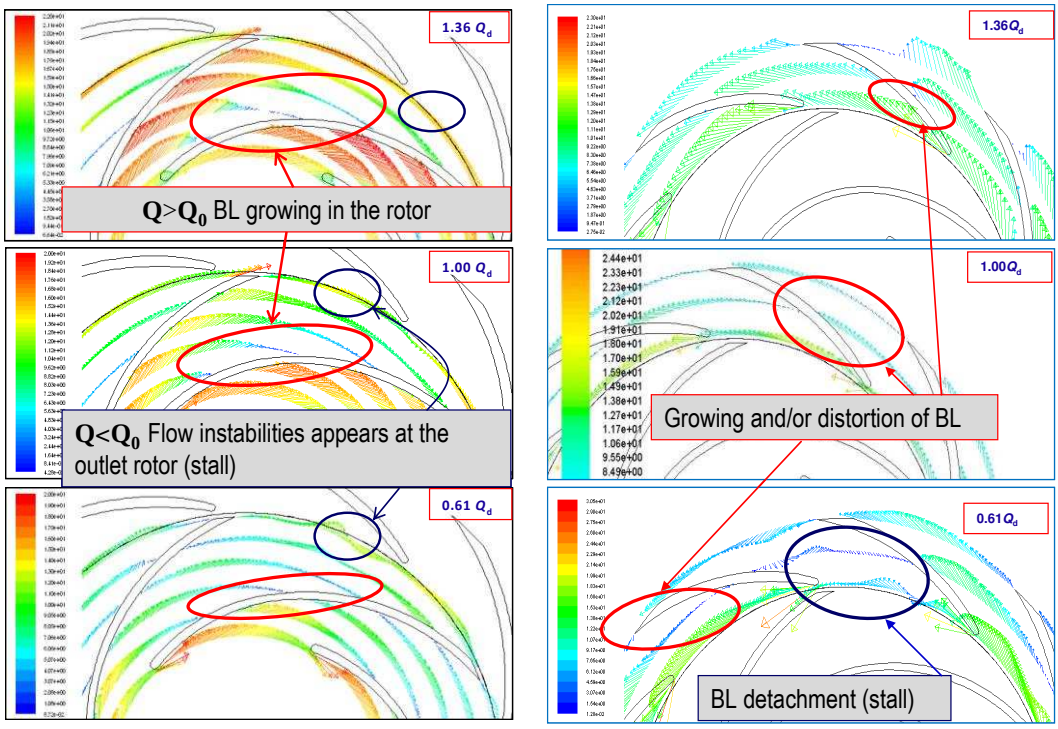

Fig.15. CFD results for the flow field under three operation conditions, vaned pump: **Left:** Flow pattern in the rotor, **Right:** Flow pattern in the diffuser (stator). **Notation: BL**, boundary Layer; $Q_0=Q_d$, Design flow rate.

A complete analysis of these stalling cycles can be performed by means of CFD. In Fig.16 the pressure fluctuations in the diffuser are presented, showing an unsteady behavior related with the 'stalling cycle' in the channel diffuser. The cycle showed is related to an equivalent time of nine cycles of the rotor blades passing at this point (i.e., t=9t*). It can also be seen that the sequence of stall/unstall appears every two diffuser channels.

For cases of low flow rates, i.e., $Q<Q_0=Q_d$, the pressure pulsations are stronger than for high flow ratios; this fact is confirmed by experimental results for hydraulic machinery working under this condition (see details in Fontanals 2012).

Finally it is necessary to remark that all the CFD results presented here, give good adjustments of the experimental results despite they are obtained in 2D geometry. The obtained results were also compared against CFD results for other 2D geometry from Feng, giving similar trends for the velocity fluctuations. The experimental measurements from Tsukamoto, were obtained in a mixed flow pump (n_q~53). It is broadly known that mixed machines have double curvature blades; therefore, the experimental machine has a full 3D geometry.

It is quite easy to obtain a 2D geometry of a turbomachine from the mean characteristics of the pump, pictures and drawings are given in the references found in the literature (e.g. see Tsukamoto et al., 1995 and Feng et al., 2011). Instead, obtaining a 3D geometry from the available data is not a trivial task, because the available experimental databases do not provide complete information of the full 3D geometry normally.

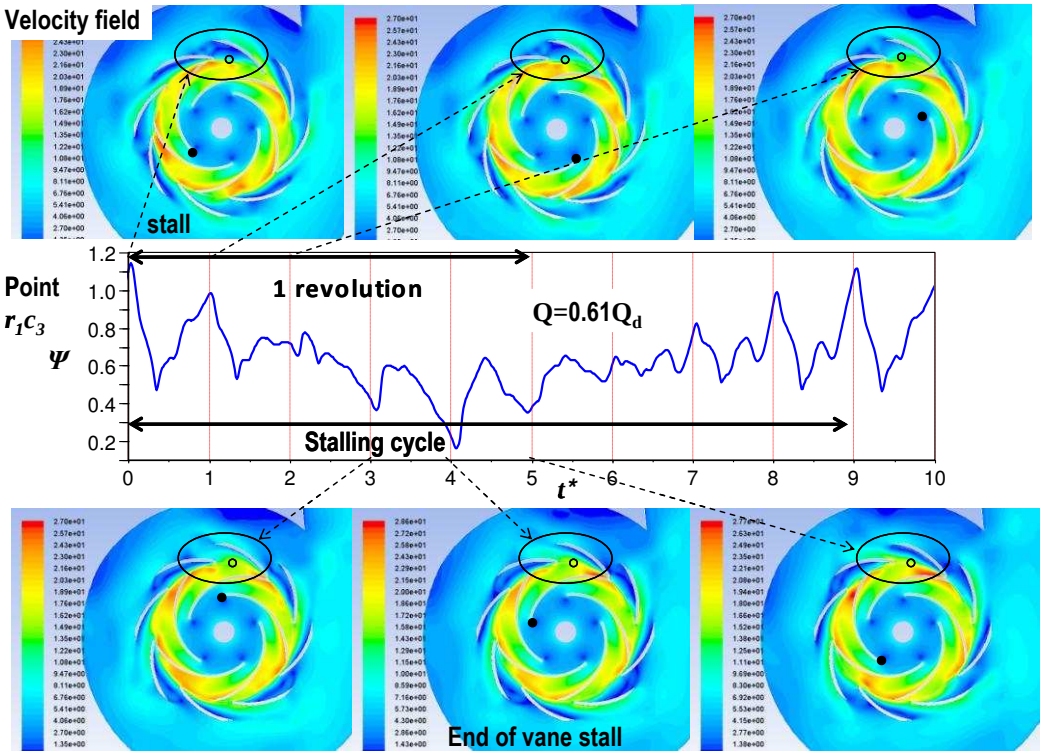

Fig.16. CFD results for velocity field and pressure fluctuations, point r_1c_3, Q/Q_d=0.61. In the sequence of pictures the stalling cycle in the stator (curve in blue) joined with the related velocity field is shown.

Despite the fact that to obtain a 3D geometry is not easy, future work will consist in 3D simulations in order to check the RSI phenomena and other fluid-structure interaction (e.g. stator-volute interaction, casing tongue-stator interaction, others).

To reach this goal, it is necessary to reconstruct the 3D geometry using the given characteristics of the machine (e.g. the experimental pump from Tsukamoto et al.,), by means of a 'classical design' of turbomachinery, (a skill not very common in the industrial engineers nowadays). To perform this reconstruction it was necessary to revisit the main concepts of the 'classical design', and a classical preliminary design was carried out to obtain the 3D geometry for this machine (see Fig.17), and the obtained 3D geometry of the rotor can be seen in Fig.18.

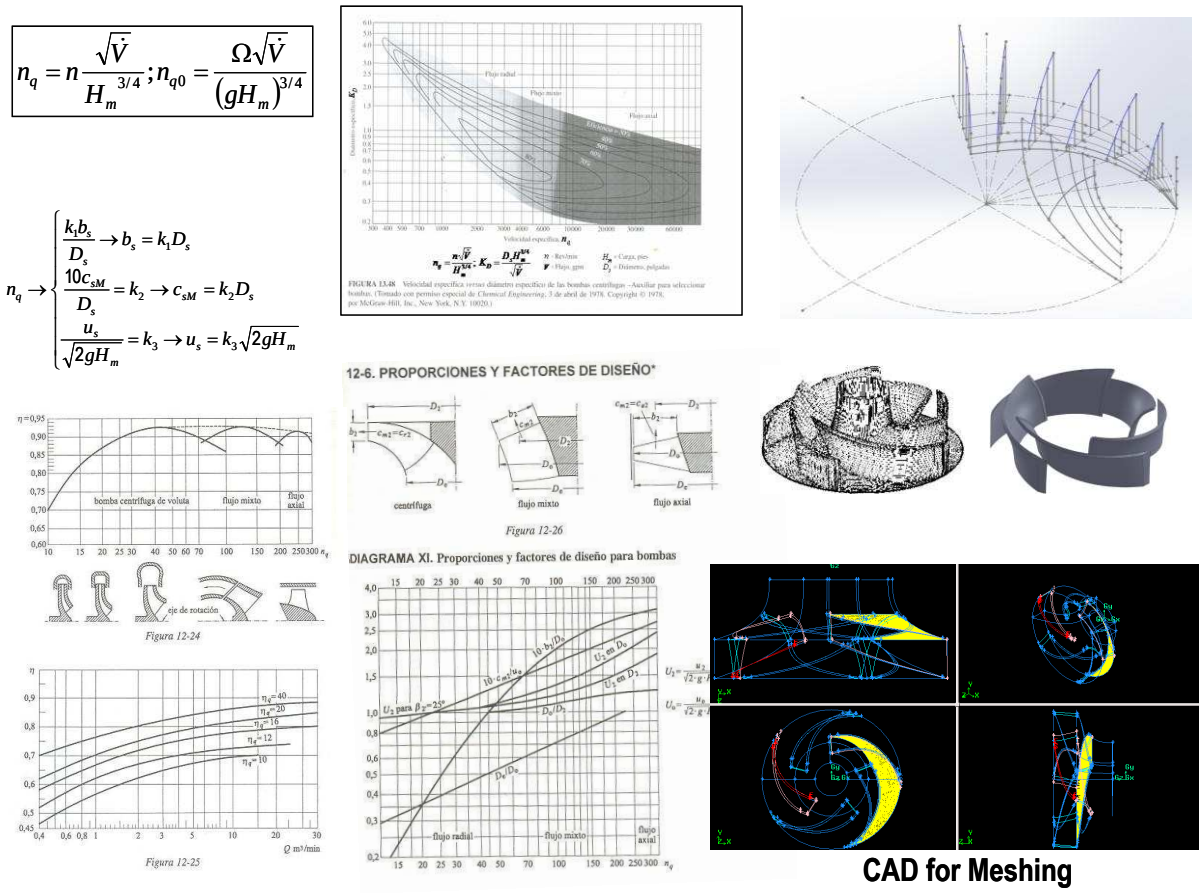

Fig.17. Summary of steps followed for obtaining a 3D rotor configuration by means of a semi-empirical 'classical design' of a mixed pump (Tables and curves are extracted from the common literature found, developed for specific undergraduated Fluid Mechanics courses).

It can be compared to the geometry used by Shi et al., 2001, in his CFD work. After completing the 3D geometry design, a line of the future work comprises the 3D simulation of the complete machine using the quantitative criteria for the assessment of internal flow state obtained in this work. Extensions of the background obtained in the turbomachinery design for reproducing the Feng et al. 2011 geometry and a subsequent comparison of the velocity field provided by experiments (unfortunately here, pressure fluctuations were not measured) will be also performed.

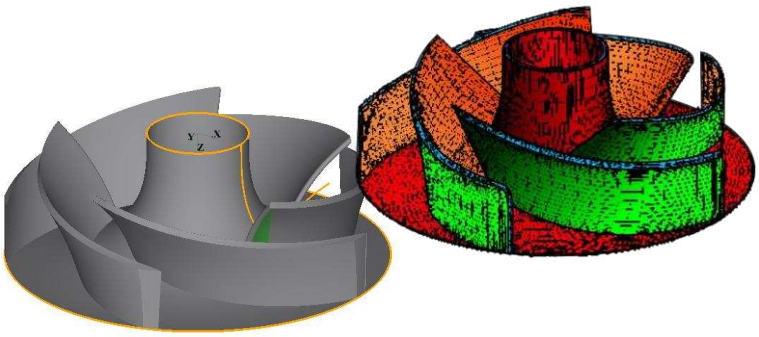

Fig.18. **Left:** Rotor configuration obtained by means of a 'classical design' of a mixed pump. **Right:** rotor configuration from Shi et al, 2001 [26].

5 CONCLUSIONS

It is known that EVMs have advantages related to CPU costs compared against other more sophisticated options (e.g. RSM, DES or LES), but it is also true that they have some known deficiencies when used for turbulent flows simulations. Then, in order to check the capabilities of the available EVM models applied to the turbulent flows simulations, a study of previous extensive validation/calibration works was performed, focused on the study of the capabilities of EVMs to capture the characteristics of the RSI phenomenon in a vaned diffuser pump.

This work proves by means of a very detailed comparison of the results obtained against experimental databases and other CFD works found in the literature, that it is possible to observe the flow instabilities due to RSI phenomenon that affect the general flow pattern when the machine works under design and off-design conditions. This information is very useful for the design engineer in order to analyse and to propose a more efficient design without carrying out several and very expensive experiments.

It was observed that the SAS modeling option improves the results obtained in some cases when it is compared with the ones obtained by means of EVMs models for meshes of similar size. This allows performing accurate unsteady simulations with lower CPU costs compared with DES/LES simulations, because DES/LES simulations need bigger meshes than SAS modeling.

Despite the promising results obtained with SAS, more intensive validation/calibration work is needed for modeling both design as well as off-design conditions using experimental databases having more complete information. At moment these databases are very scarce in the literature.

A recovering of the classical design tools was carried out for extending the 2D geometries cases towards 3D geometry ones for a more complete and accurate turbomachinery CFD modelling.

ACKNOWLDEDGEMENTS

Current work was partially supported by the Universidad Tecnológica Nacional, UTN, within its own research programme (UTN/SCTyP). Authors would like to express their appreciation to the UTN for providing financial support for this study (research projects UTI3504TC, and UTI3543TC).

REFERENCES

ANSYS Inc. ANSYS FLUENT Software, http://www.ansys.com/Industries/ Academic/Tools/, 2015.

Coussirat M. Theoretical/Numerical Study of Flows with Strong Streamlines Curvature, *PhD Thesis, Universitat Politècnica de Catalunya. Spain,* 2003.

Coussirat M., Fontanals A., Grau J., Guardo A. and Egusquiza E. CFD Study of the Boundary Layer Influence on the Wake for Turbulent Unsteady Flow in Rotor-Stator Interaction. *IAHR 24th Symposium on Hydraulic Machinery and Systems. Foz do Iguassu, Brazil,* 2008.

Coussirat M., Fontanals A. and Guardo A. CFD Study of the Rotor-Stator Interaction in a Centrifugal Pump With Diffuser. *Anales AFA Vol. 23 Fluidos (pp 34-38), Bs.As., Argentina,* 2012.

Coussirat M., Moll F., Cappa F., and Fontanals A. Study of Available Turbulence and Cavitation Models to Reproduce Flow Patterns in Confined Flows. *Journal of Fluids Engineering (in press),* 2016.

Duan L., Yuan S., Hub L., Yang W., Yu J. and Xia X. Injection Performance and Cavitation Analysis of an Advanced 250 MPa Common Rail Diesel Injector. *Int. J. of Heat and Mass Transfer* 93, pp. 388-397, 2016.

Egorov Y., Menter F., Lechner R., and Cokljat D. The Scale-Adaptive Simulation Method for Unsteady Turbulent Flow Predictions. Part 2: Application to Complex Flows. *Flow Turbulence Combust.* 85, pp. 139–165, 2010.

Feng J., Benra F. and Dohmen H. Investigation of Periodically Unsteady Flow in a Radial Pump by CFD Simulations and LDV Measurements. *Journal of Turbomachinery*, Vol 133, 2011.

Franc J. and Michel J. *Fundamentals of Cavitation.* Kluwer Academic Publ., New York USA, 2004.

Guardo A., Fontanals A. and Coussirat M. Estudio Numérico de la Interaccion Rotor Estator en el Difusor de una Bomba. *Mecánica Computacional* Vol XXXII, AMCA, pp.1155-1168, (in Spanish), 2013.

Fontanals A. Caracterització del Flux a Causa de la Interacció Rotor-Estator en Turbomàquines Mitjançant CFD. *PhD Thesis, Universitat Politètcnica Catalunya*. Barcelona, Spain (in Catalan), 2012.

Fontanals A., Coussirat M., Guardo A. and Egusquiza E. Detailed Study of the Rotor-Stator Interaction Phenomenon in a Moving Cascade of Airfoils. *IAHR 25th Symposium on Hydraulic Machinery and Systems.* Timisoara, Romania, 2010.

Fontanals A., Guardo A., Coussirat M. and Egusquiza E. Numerical Study of the Fluid–Structure Interaction in the Diffuser Passage of a Centrifugal Pump. *COUPLED PROBLEMS 2011, IV Int. Conf. on Comput. Methods for Coupled Problems in Scie. and Eng.*, 2011.

Fontanals A., Guardo A., Zobeiri A., Egusquiza E., Farhat M. and Avellan F. Boundary Layer Effects on the Vortex Shedding in a Donaldson- type Hydrofoil. *IAHR 27th Symposium on Hydraulic Machinery and Systems.* Montreal, Canada, 2014.

Kozubková M., Rautová J. and Bojko M. Mathematical Model of Cavitation and Modeling of Fluid Flow in Cone. *Procedia Engineering* 39, pp. 9–18, 2012.

Kubota A. Kato H. and Yamaguchi H. A New Modeling of Cavitating Flows: A Numerical Study of Unsteady Cavitation on a Hydrofoil Section. *J. Fluid Mech*., 240, pp. 59–96, 1992.

Li H., Kelecy F., Egelja-Maruszewski A., and Vasquez S. Advanced Computational Modeling of Steady And Unsteady Cavitating Flows. *Proceedings of IMECE2008, 2008 ASME International Mechanical Engineering Congress and Exposition.* Boston, Massachusetts, USA, 2008.

Menter F., Kuntz M. and Langtry R. Ten Years of Industrial Experience with the SST Turbulence Model, Turbulence. *Heat and Mass Transfer* 4, K. Hanjalic et al., eds., House, Inc.,

pp. 625–632, 2003.
Menter F. and Egorov Y. The Scale-Adaptive Simulation Method for Unsteady Turbulent Flow Predictions. Part 1: Theory and Model Description. *Flow Turbulence Combust.* 85, pp. 113–138.
Pedersen N., Larsen P. and Jacobsen C. Flow in Centrifugal Pump Impeller at Design and Off Design Conditions- Part I: Particle Image Velocimetry (PIV) and Laser Doppler Velocimetry (LDV) Measurements. *Journal of Fluids Engineering*, Vol. 125, 2003.
Peters A., Sagar H., Lantermann U. and Moctar O. Numerical Modeling and Prediction of Cavitation Erosion. *Wear* 338 339, pp. 189 201, 2015.
Rodriguez C., Egusquiza E., and Santos I. Frequencies in the Vibration Induced by the Rotor Stator Interaction in a Centrifugal Pump Turbine. *Journal of Fluids Engineering*, Vol.129, No. 11, pp. 1428–1435, 2007.
Sagaut P. *Large Eddy Simulation for Incompressible Flows: An Introduction*. Springer, Berlin, 2006.
Shi F. and Tsukamoto H. Numerical Study of Pressure Fluctuations Caused by Impeller-Diffuser Interaction in a Diffuser Pump Stage. *ASME J. Fluids Eng*., 123, pp. 466–474, 2001.
Singhal A., Athavale M., Li H. and Jiang Y. Mathematical Basis and Validation of Full Cavitation Model. *ASME J. Fluids Eng.* 124, pp. 617–624, 2002.
Tsukamoto H., Uno M., Hamafuku H., and Okamura T. Pressure Fluctuation Downstream of a Diffuser Pump Impeller. *The 2nd Joint ASME/JSEM Fluids Engineering Conference, Forum of Unsteady Flow*, FED-Vol. 216, pp. 133–138, 1995.
Zwart J., Gerber A. and Belamri T. Two-Phase Flow Model for Predicting Cavitation Dynamics. *Proc. 5th International Conference on Multiphase Flow*, Yokohama, Japan, paper 152, 2004.